Heart Motion Prediction Based on Adaptive Estimation Algorithms for Robotic-Assisted Beating Heart Surgery

E. Erdem Tuna, *Student Member, IEEE*, Timothy J. Franke, *Student Member, IEEE*, Özkan Bebek, *Member, IEEE*, Akira Shiose, Kiyotaka Fukamachi, and M. Cenk Çavuşoğlu, *Senior Member, IEEE*

***Abstract*—Robotic-assisted beating heart surgery aims to allow surgeons to operate on a beating heart without stabilizers as if the heart is stationary. The robot actively cancels heart motion by closely following a point of interest (POI) on the heart surface—a process called active relative motion canceling. Due to the high bandwidth of the POI motion, it is necessary to supply the controller with an estimate of the immediate future of the POI motion over a prediction horizon in order to achieve sufficient tracking accuracy. In this paper, two least-squares-based prediction algorithms, using an adaptive filter to generate future position estimates, are implemented and studied. The first method assumes a linear system relation between the consecutive samples in the prediction horizon. On the contrary, the second method performs this parametrization independently for each point over the whole the horizon. The effects of predictor parameters and variations in heart rate on tracking performance are studied with constant and varying heart rate data. The predictors are evaluated using a three-degree-of-freedom (DOF) test bed and prerecorded *in vivo* motion data. Then, the one-step prediction and tracking performances of the presented approaches are compared with an extended Kalman filter predictor. Finally, the essential features of the proposed prediction algorithms are summarized.**

***Index Terms*—Active relative motion canceling, beating heart surgery, prediction algorithm, signal estimation, surgical robotics.**

Manuscript received May 13, 2012; accepted August 29, 2012. Date of publication September 28, 2012; date of current version February 1, 2013. This paper was recommended for publication by Associate Editor M. Minor and Editor G. Oriolo upon evaluation of the reviewers' comments. This work was supported in part by the National Science Foundation under Grant CISE IIS-0222743, Grant IIS-0805495, Grant IIS-0905344, and Grant CNS-1035602; the National Institutes of Health under Grant R21 HL096941; and Case Western Reserve University, with a Support of Undergraduate Research and Creative Endeavors award. This paper was presented in part at the the IEEE International Conference on Intelligent Robots and Systems, San Diego, CA, 2007, and the IEEE International Conference on Robotics and Automation, Pasadena, CA, 2008.

E. E. Tuna, T. J. Franke, and M. C. Çavuşoğlu are with the Department of Electrical Engineering and Computer Science, Case Western Reserve University, Cleveland, OH 44106 USA (e-mail: eet12@case.edu; tjf6@case.edu; cavusoglu@case.edu).

Ö. Bebek was with the Department of Electrical Engineering and Computer Science, Case Western Reserve University, Cleveland, OH 44106 USA. He is now with the Department of Mechanical Engineering, Özyeğin University, Istanbul 34662, Turkey (e-mail: ozkan.bebek@ozyegin.edu.tr).

A. Shiose was with the Department of Biomedical Engineering, Lerner Research Institute, Cleveland Clinic, Cleveland, OH 44195 USA. He is now with the University of Pittsburgh Medical Center, Pittsburgh, PA 15213 USA (e-mail: as-1@heart.med.kyushu-u.ac.jp).

K. Fukamachi is with the Department of Biomedical Engineering, Lerner Research Institute, Cleveland Clinic, Cleveland, OH 44195 USA (e-mail: fukamak@ccf.org).

Color versions of one or more of the figures in this paper are available online at http://ieeexplore.ieee.org.

Digital Object Identifier 10.1109/TRO.2012.2217676

I. Introduction

CORONARY artery bypass graft (CABG) surgery requires surgeons to operate on blood vessels that move with high bandwidth. This rapid motion of the heart makes it difficult to track these arteries by hand effectively [1]. Contemporary techniques either stop the heart and use a cardio-pulmonary bypass machine, *on pump*, or passively restrain the beating heart with mechanical stabilizers, *off pump*, in order to cancel the biological motion of heart during CABG surgery. However, using on-pump CABG surgery might cause the patient to suffer from long-term cognitive loss due to possible complications as a consequence of stopping the heart [2]. Off-pump CABG surgery is limited to the front surface of the heart and significant residual motion is observed during stabilization [3].

Robotic-assisted beating heart surgery replaces the conventional surgical tools with robotic instruments, which are directly controlled by the surgeon through teleoperation. The surgeon views the surgical site through a camera mounted on a robotic arm that follows the heart motion, showing the surgeon a stabilized view [4]. A surgical robot, which moves simultaneously with the heart, is used to track and cancel the relative heart motion. Thus, the surgeon operates on heart as if it is stationary. This approach is called "active relative motion canceling (ARMC)." This would eliminate the use of cardio-pulmonary bypass machine (the pump) and prevent shortcomings of the on-pump CABG surgery. It differs from the traditional off-pump CABG surgery since in the proposed robotic-assisted surgical system, heart motion is canceled with motion compensation [5].

The relatively fast and high-bandwidth motion of a point of interest (POI) on the heart surface establishes challenging requirements for motion tracking with high precision [6]. The surgeon is required to operate on blood vessels whose diameters vary from 0.5 to 2 mm and have a quasi-periodic motion at the rates of 1–2 Hz. In order to perform precise operations on these vessels, root-mean-square (RMS) position tracking error of the POI has to be in the order of 100–250 μm. Causal error feedback control alone is not able to reduce the tracking error sufficiently. A predictive controller which implements a receding horizon model predictive control (RHMPC) in the feedforward path was found to be necessary [7], [8].

The primary goal of this research is to improve the tracking performance of a surgical robot prototype as proof of concept that the motion cancelation can be achieved. To this end, the tracking performance research has primarily been focused on developing estimation methods for use with an RHMPC. Such a predictive controller needs an estimate of the future POI motion. The estimate needs to be of a finite duration into the future, which is referred to as the prediction horizon.

In this paper, heart motion prediction methods based on adaptive filtering techniques are studied. The implementations parameterize a linear system to predict the POI motion and rely on recursive least-squares (RLS) adaptive filter algorithms. The presented methods differ as the first one assumes a linear system relation between the consecutive samples in the prediction horizon, whereas the second method performs the parametrization of the linear system independently for each point throughout the horizon. The presented one-step adaptive filter and the generalized adaptive filter were initially proposed by Franke *et al.* in [9] and [10], respectively. The analysis of these predictors are extended in this paper. In the literature, these predictors were tested with very limited and short duration of constant heart rate data. During the course of this research, these two algorithms are exhaustively studied with a wide range of different prerecorded *in vivo* constant and varying heart rate motion data. The effectiveness and feasibility of these algorithms are studied by simulations and evaluated on a three-degree-of-freedom (DOF) hardware.

The rest of this paper is organized as follows. Related works in the literature are described in Section II. In Section III, experimental heart motion data are analyzed. Problem formulation is explained in Section IV. Sections V and VI describe the prediction methods and discuss how the methods differ from each other to create estimations throughout the prediction horizon. Implementation details are addressed in Section VII. In Section VIII, simulation and experimental results are given. Finally, the discussion and conclusions are presented in Sections IX and X, respectively.

II. Related Works in the Literature

This paper is concerned with estimating the prediction horizon for RHMPC—a control scheme that relies on the estimate of the prediction horizon as a reference signal. There are several research groups that have already studied and proposed ways to estimate the POI motion on the heart surface.

Ortmaier *et al.* [11] used Takens Theorem to develop a robust prediction algorithm, anticipating periods of lost data when a tool obscured the visual tracking system. Estimates were generated from a linear combination of embedding vectors of previous heart data. The weights were chosen such that better estimating vectors are weighted more heavily. The algorithm had a global prediction technique that correlated ECG signals to heart motion. It was able to estimate the system behavior when visual contact of the landmark was lost for some period of time.

Ginhoux *et al.* [8] separated breathing motion from heart motion in the prediction algorithm. The breathing motion was treated as perfectly periodic, since the patient would be on a breathing machine. The heart motion was predicted by estimating the fundamental frequency, as well as the amplitude and phase of the first five harmonics. This prediction was used to estimate disturbance so that the controller could correct for it.

Rotella [7] used the previous cycle of heart motion data as an estimate of future behavior. This led to problems since the POI motion was not perfectly periodic. Bebek and Cavusoglu [5] improved upon this prediction scheme by synchronizing heart periods using ECG data and separated heart and breathing motion, predicting only heart motion. Bebek noted that the prediction method still could be improved.

Bader *et al.* [12] presented a model-based approach for reconstructing the position of any arbitrary POI and for predicting the heart's surface motion in the intervention area. They modeled the POI motion by means of a pulsating membrane model. The membrane motion was described by means of a system of coupled linear partial differential equations (PDEs) and obtained a bank of lumped systems after spatial discretization of the PDE solution space by the finite spectral element method. A Kalman filter was employed to estimate the state of the lumped systems by incorporating noisy measurements of the heart surface.

Richa *et al.* [13] implemented and compared the Fourier-series and vector autoregressive models that were used in the literature to estimate the immediate future of a POI. They employed extended Kalman filter (EKF) as the recursive estimation algorithm for both models. More recently, Richa *et al.* [14] proposed a dual time-varying Fourier series motion model, which models the heartbeat and breathing components of the heart motion explicitly. They used an EKF to estimate the model parameters recursively. The presented model was used to predict future heart motion for bridging tracking failures and reestablishing tracking POI motion in case of occlusions.

Batcha *et al.* [15] classified and reviewed existing prediction algorithms in the literature and proposed a prediction technique based on amplitude modulation (AM). They took into account of the coupling between the breathing and heartbeat components of heart motion and expressed the cardiac motion as a sum of a breathing component and an amplitude modulated heartbeat component. Breathing component, carrying and modulating signals of the AM heartbeat component were represented by a Fourier-series model. Only the first low-frequency heartbeat harmonics were modulated and heartbeat component was reparametrized by this modulation. The parameters of the developed model were estimated by a RLS algorithm.

Yuen *et al.* [16] developed a 1-DOF ultrasound-guided motion compensation system for cardiac surgery. The surgical system integrates 3-D ultrasound imaging and a robotic instrument with a predictive controller that compensates for the 50–100-ms imaging and image processing delays to ensure good tracking performance. Yuen *et al.* [17] used EKF algorithm to predict the future position of mitral valve annulus motion. The EKF filter was used to feedforward the trajectory of a cardiac target in order to compensate time delays occurred due to the acquisition of motion data by the 3-D ultrasound imaging. They tested the performance of EKF in prediction and tracking in the presence of high measurement noise and heart rate variability. They

reported RMS synchronization errors of 1.5 mm for trajectories derived from clinical heart rate variability data.

This paper studies new estimation algorithms into the controller described in the earlier work of Rotella [7] and Bebek and Cavusoglu [5]. Two novel prediction techniques using adaptive filters are presented which were originally described by Franke *et al.* in [9] and [10]. The presented approaches are used in place of the prediction algorithm of Bebek and Cavusoglu [5]. Since the new predictors are parameterized by a least-squares algorithm, the predictors are inherently robust to noise. The predictors only use recent past and present observations making them less susceptible to differences between heart periods than the algorithm of Bebek and Cavusoglu [5]. Although Ginhoux *et al.* [8] formulated prediction for periodic POI motion, no assumptions are made *a priori* in this study toward periodicity of the system, rather the predictors are unconstrained so that they can best mimic the POI motion. This is the first study that uses real varying heart rate data to perform heart motion tracking.

In the following sections, tracking and prediction performance of the adaptive are predictors presented, and they are compared with the EKF predictor used in the study of Yuen *et al.* [17].

III. Analysis of Heart Data

In this section of the paper, experimental setup for the data collection is explained. Varying heart rate motion data collected via this setup are further analyzed. Data were collected from three calves and all the study was performed with on bench-top with these prerecorded data. From each calf, a duration of 736 s, 472 s, and 340 s of data was processed and used in this study.

A. Experimental Setup for Measurement of Heart Motion

The prerecorded data used in this study were collected using a sonomicrometry system (Sonometrics Inc., ON, Canada). The sonomicrometry system has also been the sensor of choice in our previous work for measuring heart motion for robotic ARMC [5]. A sonomicrometer measures the distances within the soft tissue via ultrasound signals. A set of small piezoelectric crystals attached to the tissue while heart is still beating. These crystals are used to transmit and receive short pulses of ultrasound signal, and the "time of flight" of the sound wave as it travels between the transmitting and receiving crystals is measured. Using these data, the 3-D configuration of all the crystals can be calculated [18]. Absolute accuracy of the sonomicrometry system is 250 μm (approximately a one-fourth wavelength of the ultrasound) [19].

In the experimental setup, one crystal of the sonomicrometry system was sutured on the heart while heart was beating. While collecting measurements, this crystal on the heart was placed in two different locations. The first location, which is referred to as "Top" in the rest of the paper, was located on the front surface. Specifically, the sonomicrometry crystal was placed at 1 cm laterally from the left anterior descending coronary artery and 8 cm cranially from the left ventricular (LV) apex. The second location, which is referred to as "Side," was the location on the side surface of the heart. Specifically, in this case, the crystal was placed at 5 cm laterally from the left anterior descending coronary artery and 10 cm cranially from the LV apex. Five other crystals were asymmetrically mounted on a rigid plastic base of diameter 60 mm, on a circle of diameter 50 mm, forming a reference coordinate frame. This rigid plastic sensor base was placed in a rubber latex balloon, which was filled with a 9.5% glycerine solution. The reason of using such a setup was to ensure a continuous line of sight between the base crystals and the crystal on the heart surface through a liquid medium for proper operation of sonomicrometry sensor system. Fig. 1 shows the experimental setup for measurement of heart motion. The sonomicrometer crystals that are sutured on the heart can be seen from the figure. The pacemaker leads that are used to change the heart rate and the sonomicrometer base are also visible.

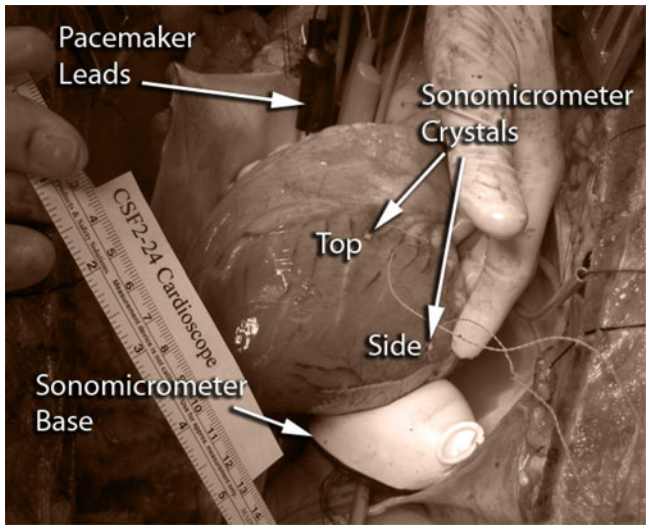

Fig. 1. Two sonomicrometer crystals that are sutured on the anterior and posterior surfaces of the heart are used for data collection. Pacemaker leads and sonomicrometer base are also visible in the image.

Data were processed offline using the proprietary software provided with the system to calculate the 3-D POI motion. The only filtering performed on the data produced by the sonomicrometry system was the (very limited) removal of the outliers, which occasionally occur as a result of ultrasound echoing effects. Although the sonomicrometry system can operate at 2-kHz sampling rate for measuring the location of the POI crystal relative to the fixed base, in our test experiments, we have collected data at sampling rates of 257 and 404 Hz in order to collect redundant measurements.

B. Analysis of Varying Heart Rate Motion Data

The motion of the heart surface is quasi-periodic in nature. The POI motion on the heart is primarily the superposition of two effects: motion due to heart beating and motion due to breathing. Each of these signals closely resembles periodic signals.

In practice, the statistics of heart motion is likely to change during surgery. Such a change would result in variations in the underlying dynamics of the POI's motion. In order to explore the effects of these slow variations on the tracking performance and investigate how the adaptive algorithms will adjust to these

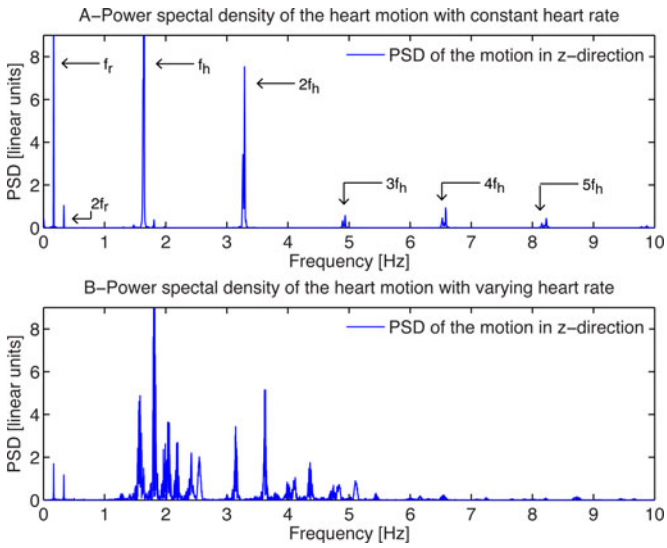

Fig. 2. Power spectral density (PSD) of the heart motion in the z-direction. (A) PSD of heart motion with constant heart rate. Tall, narrow peaks with the absence of intermittent frequencies indicate largely periodic motion of the heart. (B) PSD of heart motion with varying heart rate.

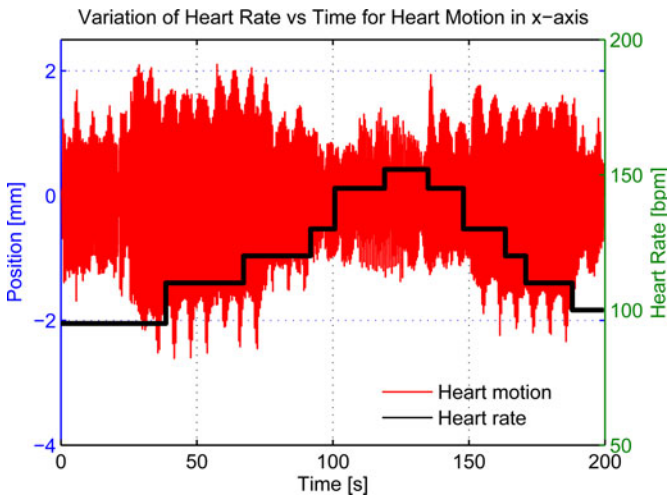

Fig. 3. Variation of heart rate with respect to time for the heart motion in x-direction. An artificial pacemaker is used to vary heart rate while collecting data.

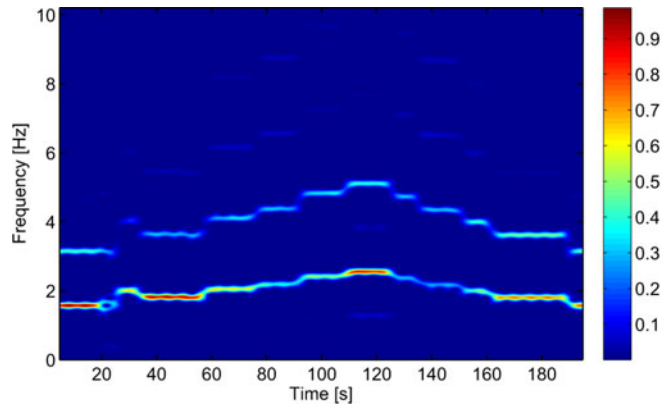

Fig. 4. Frequency spectrum of the z-component of 3-D varying heart rate motion. Color mapping on the right corresponds to the intensity values of the frequency components.

changes, two distinct types of experimentally collected heart data are used in this study. In the first type, heart rate is constant whereas it is varying in the second type.

Fourier analysis of the heart signal data with constant heart rate reveals how this periodic nature is prevalent [see Fig. 2(A)]. The first peak corresponds to lung motion, which is estimated by filtering the heart motion data using a low-pass Equiripple FIR filter of cutoff frequency 1.0 Hz. It has a fundamental frequency of approximately 0.17 Hz, f_r, with first harmonic at 0.33 Hz is appearing significant. The heart motion itself has a fundamental frequency f_h of 1.66 Hz, corresponding to 100 beats/min, with the first four harmonics clearly visible in the figure. The POI motion has a broader bandwidth and can be approximated with an error less than 140 μm RMS with frequency components up to 26 Hz. These results are consistent with the heart motion measurements reported by Groeger *et al.* [20]. The peak-to-peak amplitude of the POI motion is 8.39 mm, with a RMS value of 3.55 mm. The sharpness of these peaks indicates that the harmonics decay very little in time, meaning that the overall motion of the POI is similar to a superposition of periodic signals.

In order to change the heart rate, an artificial pacemaker was employed which uses electrical impulses to regulate heart rate, generated by electrodes contacting the heart muscles. Initially heart was allowed to beat for 40 s at 95 beats/min. Then, the heart rate was gradually increased from 95 to 152 beats/min by approximately 10 beats/min steps and then decreased in the same way, where heart was allowed to beat for at an average 15 s at a particular heart rate. Fig. 3 shows the variation in heart rate with respect to time for the heart motion in the x-direction. Additionally, a spectral analysis of the data is presented in Fig. 4, which shows the spectrogram of the z-component of varying heart rate motion data. Variations in the heart rate through data duration can be evaluated from the spectrogram, which are consistent with Fig. 3. The maximum frequency is adjusted to 10 Hz for a clear frequency resolution and harmonic representation. The spectrogram is obtained by computing a fast Fourier transform (FFT) using a Hanning window.

In the Fourier analysis of varying heart rate data, Fig. 2(B), the first observable dominant mode at 0.17 Hz corresponds the breathing motion, similar to constant heart rate data, with a significant first harmonic at 0.33 Hz. The remaining motion due to the beating of heart shows the fundamental frequencies of heart motion for different heart rates. The peaks at 1.58, 1.81, 2.03, 2.18, 2.42 and 2.54 correspond to a heart rate of 95, 110, 120, 130, 145, and 152 beats/min, respectively. The peak-to-peak amplitude of the POI motion is 7.43 mm, with an RMS value of 3.38 mm.

IV. Problem Formulation

The control algorithm establishes the most essential part of the robotic tools for tracking heart motion during CABG surgery. As explained in Section III, low-frequency components of heart motion result from breathing and high-frequency components correspond to the heartbeat component. Breathing motion can be

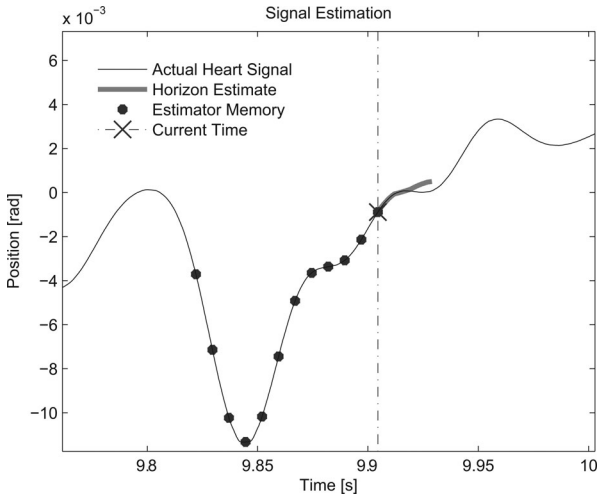

Fig. 5. Schematic of the prediction problem. The circles represent past observations, now in memory, the "X" is the current observation, and the short curve originating from there is the horizon estimate. The predictor takes the past observations and produces the horizon estimate from past observations.

easily canceled by using a purely feedback controller due to its low bandwidth. However, rapid motion of heartbeat component possesses demanding requirements on the control architecture in terms of the bandwidth of the motion that needs to be tracked. This necessity resulted in utilizing a feedforward algorithm in the control architecture in order to cancel high frequency components of the heart motion after the breathing motion is filtered out. In this study, an RHMPC (originally developed in [5]) was employed as the feedforward control algorithm, requiring an estimate of the immediate future of the POI motion. If the feedforward controller has high enough precision to perform the necessary tracking, then the tracking problem can be reduced to predicting the estimated reference heartbeat signal effectively [5].

The following notation will be used for formulating the motion estimation problem. Let z_i represent an observation at time i. In this case, z_i is a 3-D column vector representing the location of the POI in Cartesian coordinates. At a given time step n, the observation z_n indicates the current 3-D position of the heart. Then, the observation z_{n-1} represents the previous position of heart, and the older observations are referenced by decreasing subscript index, e.g., z_{n-5} is the observation from five samples ago. In a similar fashion, z_{n+1} represents the next observation. Yet, this observation has not occurred, and will not be known until it becomes the present value. The estimate for the next observation is introduced as $\hat{z}_{n+1}$.

Using this notation, the prediction problem can be posed as follows: Given the N-dimensional vector of known samples leading up to time n, $[z_n, z_{n-1}, \ldots, z_{n-N+1}]^T$, find the best estimate of the M-dimensional horizon $[z_{n+1}, z_{n+2}, \ldots, z_{n+M}]^T$. Fig. 5 provides a graphical schematic of this problem. The best estimate is defined to be the one that minimizes the square of the estimation error, where the estimation error is the difference between the prediction and the observed value at that time. Once a method is established to predict the next observations, a sequence of future observations can be estimated.

Two adaptive filter-based motion estimation algorithms are presented in this paper to estimate reference heartbeat signal, namely one-step adaptive filter-based motion estimation algorithm and a generalized adaptive filter-based motion estimation algorithm. These two methods formulate and then parameterize the model of heart motion differently as described in Sections V and VI.

V. One-Step Motion Estimation Algorithm

The POI motion is a continuous-time dynamic system (see Section IV). To establish a method for predicting future positions of POI, an equivalent discrete-time system has to be used. Yet, neither the state space nor the dimension of the heart is obvious. Therefore, to simplify the prediction method, a finite and low-order state vector must be employed in the heart model. The quasi-periodic nature of heart motion (see Section III) allows the state transition function to be approximated as linear by the following intuition.

The sharpness of the peaks of significant harmonics indicates that the harmonics decay very little in time, meaning that the overall motion of the POI is similar to a superposition of periodic signals [see Fig. 2(A)]. Therefore, for the constant heart rate motion data, a linear system can easily be constructed, which has a frequency response that mimics the heart signal's Fourier representation. The transient response would then resemble the observed heart data. Thus, given the current state of the actual heart signal as initial values for the system, the transient response would follow the actual heart motion−giving a prediction. Yet, it is important to note that this linear system modeling is not valid for the varying heart rate motion data [see Fig. 2(B)].

Finally, if the state was formulated as a stacked vector of past observations, then the determination of the initial state would be trivial. A linear system of the aforementioned specifications would meet the requirements for the heart model transition function. However, the model would still need to be parameterized in a way to statistically minimize the error of the prediction.

A. Model of Heart Motion

The heart position data consist of 3-D vectors representing position. These vector samples are assumed to be generated from a vector autoregressive model (VAR). A VAR process has multiple output signals that are correlated with each other. The model which establishes the heartbeat component of heart motion is given by the following equation [21]:

$$\vec{z}_k = \sum_{i=1}^{N} A_i \vec{z}_{k-i} + \vec{\gamma}_k. \tag{1}$$

In this case, it is an Nth-order VAR model. Each observation is given by a weighted sum of past observations, and is perturbed by noise given by $\vec{\gamma}_k$. Noise vector $\vec{\gamma}_k$ is assumed to be zero mean white noise. Since the linear combination of past observations account for correlation between observations, for any two noise vectors $\vec{\gamma}_k$ and $\vec{\gamma}_i$, $\vec{\gamma}_k$ is uncorrelated with $\vec{\gamma}_i$ for $i \neq k$. Since the noise vector is assumed to be white, it is not useful when generating predictions of future values. Therefore, when

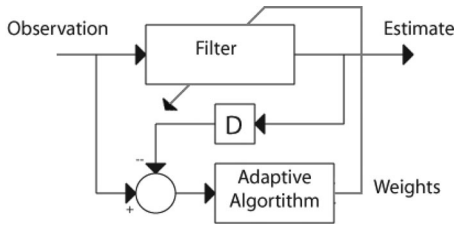

Fig. 6. Adaptive filter is arranged to minimize the error between the estimate for the current observation, calculated in the last iteration, and the actual observed value. This way, the weights of the filter are statistically optimized to estimate one step ahead.

parameterizing the equation for the purpose of prediction, only the weighting matrices need to be estimated.

The VAR model given in (1) can be reformulated in state-space canonical form as follows:

$$\vec{X}_k = \Phi \vec{X}_{k-i} + \Gamma \vec{v}_k$$
$$\vec{\sigma}_k = C\vec{X}_k. \tag{2}$$

This system can be reformulated using an arbitrary state vector; however, a stacked vector of past observations simplifies the determination of the initial state, parametrization of the state transition matrix Φ, and generation of the prediction horizon. In this case, Φ is in canonical form and can be written as

$$\Phi = \begin{bmatrix} A_1 & A_2 & \cdots & A_N \\ I & 0 & \cdots & 0 \\ 0 & I & & \vdots \\ \vdots & & \ddots & 0 \end{bmatrix}. \tag{3}$$

Future observations of the system are given by solving the state space solution at time n. In order to find the expected trajectory, we take the expectation of (2) and find that the solution takes the form

$$E\{z_{n+k}\} = C\Phi^k \vec{X}_n \tag{4}$$

where the aforementioned formula gives the horizon estimate made at time n for a value k steps into the future. Note that since Φ^k is only computed for $k < M$, where M is the horizon length, Φ^k always remains finite. Therefore, stability of Φ is not a concern. Since $\vec{v}$ is unknown, but its expected value is zero by construction, it does not appear in the solution to the expected trajectory.

B. Parametrization

Traditional system identification problems using adaptive filters arrange the filter such that the input to the filter is the system's input and the desired response is the system's desired response. This way, the filter converges toward an approximation of the system's input–output relation. However, (2) is driven by white noise input vector $\vec{v}$. This input is unknown and unable to be predicted for future observations. Thus, deriving an input–output relationship for the heart motion would be impractical. Instead, the adaptive filter is arranged as a one-step predictor (see Fig. 6). The desired response is the heart position's current observation, and the input to the adaptive filter is the previous heart observations. The adaptive filter adjusts its filter weights such that it generates the statistically best estimate for the next observation, given only the current and past observations.

In order to generate the predictions, the coefficient matrices A_i, from (1) and, equivalently, the matrix Φ from (2) need to be estimated. The state transition matrix Φ is in controllable canonical form; therefore, estimating A_i is sufficient to parameterize the estimated state transition matrix denoted by $\hat{\Phi}$. As can be seen from (1), the matrices A_i correspond to tap weights in a transversal filter. In a one-step predictor, when it has converged to a solution, its filter weights are precisely the matrices needed to parameterize $\hat{\Phi}$. This way, the adaptive algorithm estimates the matrix $\hat{\Phi}$.

C. Recursive Least Squares

RLS is chosen as the adaptation algorithm to update the filter weights. RLS is a method that updates a least-squares solution when a new piece of data is added. In practice, the RLS solution would approach the actual solution, even if the initial estimates for the solution were wrong. To formulate the RLS algorithm for vector samples, the one-step prediction problem needs to be stated as a least-squares problem

$$[z_{n-1}^T z_{n-2}^T \cdots z_{n-N}^T]\, W^T = z_n^T \tag{5}$$

where the objective is to find W such that the square of the error between the two sides of the equation is minimized. At any time step, z_n is the current position of POI, and $[z_{n-1}^T z_{n-2}^T \cdots z_{n-N}^T]$ is the N-dimensional vector of past positions. From this representation, it is clear that

$$W = [A_1\ A_2\ \cdots\ A_N] \tag{6}$$

where A_i are the weighting matrices from (1).

Using the statement of the least-squares problem for the one step estimator in (5), the RLS algorithm can be derived. The derivation of the vector-valued RLS algorithm is analogous to Haykin's derivation of the scalar case [22]. Since W is updated at every time step, the estimator is able to adapt to slowly changing heart behavior.

If the adaptive algorithm is able to forget the past, just as it would be able to converge to a stationary signal, it can track a signal with changing statistics [22]. Accordingly, the RLS algorithm is formulated with past observations exponentially windowed. The exponential window parameter λ is multiplied to each observation at each iteration, such that more recent observations carry more weight. Thus, least-squares solution places a greater importance on minimizing error for the more recent observations and their prediction than on older ones, i.e., $\lambda < 1$ [22].

From the combination of weighted memory and convergence to the optimal solution, if the statistics of the heart motion change in time, the RLS algorithm is able to adapt to the new heart behavior and the filter can track the ideal time-varying solution.

D. Prediction

Following from (4), the one-step prediction is

$$W \begin{bmatrix} z_n \\ z_{n-1} \\ \vdots \\ z_{n-N+1} \end{bmatrix} = \hat{z}_{n+1}. \tag{7}$$

Once W is determined by (6), the stacked vector of past observations is shifted down by one observation size and making the first past observation the current position z_n. Then, by matrix multiplication, the one-step prediction $\hat{z}_{n+1}$ on the horizon is computed, which is precisely the expected value of z_{n+1} from (1).

The prediction horizon of length M starting at time n is the solution to (4) with initial condition vector being the stacked vector of the past N observations.

In the actual implementation, predictions over the horizon length are generated by iterating this function several times. This avoids the computational complexity of calculating Φ^k and using it directly to compute the predictions. The calculation of $\vec{X}_n = \Phi \vec{X}_{n-1}$ is simplified by calculating $\hat{z}_{n+k}$ by (7), shifting the stacked observation vector $\vec{X}$ down by one observation size and making the first observation the current estimate. This way, the computational complexity of iterating the state variable increases proportional to N, as opposed to N^2. Since the observation matrix C from (2) simply retrieves the first observation from $\vec{X}$, multiplication by C is not necessary because the observation can be directly indexed and removed.

This recursive relationship can be written explicitly. If W is factored as $W = C\Phi_{0,1}$, where

$$\Phi_{0,1} : [z_n, \ldots, z_{n-N+1}]^T \rightarrow [\hat{z}_{n+1}, z_n, \ldots, z_{n-N+2}]^T$$
$$C : [z_n, \ldots, z_{n-N+1}]^T \rightarrow z_n; \;\; C = [I \;\; 0 \;\cdots\; 0]$$

then it is possible to define a matrix U such that it maps the memory of past observations to the expected horizon. In this case

$$U = \begin{bmatrix} C\Phi_{0,1} \\ C\Phi_{0,1}^2 \\ \vdots \\ C\Phi_{0,1}^M \end{bmatrix}$$

$$U : (z_n, z_{n-1}, \ldots, z_{n-N+1}) \rightarrow (\hat{z}_{n+1}, \hat{z}_{n+2}, \ldots, \hat{z}_{n+M}). \tag{8}$$

Using the aforementioned described method for obtaining an estimate, the horizon is generated by collecting the next M estimates of the POI trajectory. Each time the process starts, the current state vector is composed of $N-1$ past observations together with the current observation. The first one-step prediction is generated by this state vector. Then, the state vector is shifted down by one observation size and the new prediction is used as the current observation. By following this procedure, the next M estimates in the prediction horizon are generated. This collection of M estimates is the expected POI trajectory given the $N-1$ past observations and the current observation. In order to generate the next prediction horizon at the following time step, the aforementioned procedure is applied to the new state vector, where the new state vector is composed of the new actual heart position data and corresponding $N-1$ past observations.

VI. Generalized Linear Prediction

In Section V, the optimal linear one-step predictor, in the sense of prediction error magnitude, is formulated and used recursively to generate predictions. This method approximates the heart dynamics as being a linear discrete time system. In the generalized prediction method that is explained in this section, the assumption of a linear system relation between consecutive time samples is abandoned. Instead, a linear estimator for each point in the horizon is independently estimated. This is done by extending (7) as follows:

$$V \begin{bmatrix} z_n \\ z_{n-1} \\ \vdots \\ z_{n-N+1} \end{bmatrix} = \begin{bmatrix} \hat{z}_{n+1} \\ \hat{z}_{n+2} \\ \vdots \\ \hat{z}_{n+M} \end{bmatrix} \tag{9}$$

where V is the estimation matrix that maps from the collection of observations to the expected horizon. In the same way as W was parameterized, RLS is used to determine V online and adaptively. However, since (9) contains the estimated values that are being solved for, it is unsuitable for implementation via RLS as is. This can be solved by assuming POI statistics to be stationary, or at least slowly varying, which makes V approximately constant. The assumption of time invariance of the heart statistics is utilized to introduce M delays so that all quantities have been observed when solving for V

$$V \begin{bmatrix} z_{n-M} \\ z_{n-M-1} \\ \vdots \\ z_{n-N-M+1} \end{bmatrix} = \begin{bmatrix} z_{n-M+1} \\ z_{n-M+2} \\ \vdots \\ z_n \end{bmatrix}. \tag{10}$$

The analogy can be made between (10) and an adaptive filter. The right-hand side is the desired output, and the observation vector on the left-hand side is the input. Further, introducing the estimation matrices

$$\Phi_{0,i} : [z_n, \ldots, z_{n-N+1}]^T \rightarrow [\hat{z}_{n+i}, \hat{z}_{n+i+1}, \ldots, \hat{z}_{-N+n+i}]^T$$

for $1 \leq i \leq M$, V can be decomposed similar to U in (8) as

$$V = \begin{bmatrix} C\Phi_{0,1} \\ C\Phi_{0,2} \\ \vdots \\ C\Phi_{0,M} \end{bmatrix}. \tag{11}$$

The generalization of this prediction method results from the fact that, unlike in (8), $\Phi_{0,i}$ are parameterized independently and not, in general, equal to $\Phi_{0,1}^i$. The predictor is implemented in a similar way to the previous vector RLS adaptive filter. The adaptive filter is formulated to solve the delayed estimation (10). This is equivalent to using a bank of n-step predictors

but is more computationally efficient. The largest cost in the RLS algorithm involves updating the inverse covariance matrix of the inputs. The generalized predictor is an improvement on to the one-step predictor, since in generalized predictor each estimate is using the same input vector. As a result, the update of state vector only needs to be done once, providing a dramatic reduction in computational complexity of one-step predictor when predictions are being made at many points throughout the horizon.

VII. Implementation Details

A. Correlation Between Signals

The one-step prediction method described in Section V for generating estimates uses the matrices A_i as weights for the vector observations. This allows for motion along one axis to be correlated with motion on the other two. This feature comes at a significant computational cost. A less computationally intense method would be to treat motion of the POI on each axis as being independent and using a predictor of the same order for each individual axis. Since it would use three scalars to weight each past data sample, as opposed to a 3×3 matrix, it would require one-third of the computational effort to process the same number of past observations. This would allow, in a single-time step, for more samples of past data to be processed when generating the next prediction.

In order to decide which option is best for implementation, the effectiveness of each estimate per the computational effort needs to be determined. In the independent predictor, computational complexity is equivalent to the order of the adaptive filter used for the three independent RLS predictors for each individual axis. On the other hand, for the correlated predictor, the computational complexity is equivalent to the three times the order of adaptive filter used. The reason is a 3×3 matrix is used to weight each past sample instead of three scalars, which is the case in the independent predictor.

A simulation study is performed in order to test these two different options, where only prediction performances are compared. For both correlated and independent predictors, the simulation was done by using a 56 s prerecorded constant heart rate data which were processed at a sampling rate of 257 Hz. Each predictor generated the one-step prediction for each sample of the heart data and the average magnitude error is calculated between the actual data and the predicted data. The average magnitude error is shown for both systems in Fig. 7. The first x-axis located at the bottom of the plot shows the order of the correlated predictor. The second x-axis located at the top of the plot shows the order of the independent predictor. The axes are scaled such that filters with same computational complexity are aligned to have same abscissa.

The results in Fig. 7 show that treating the heart signals as being correlated yields better estimates when the computation effort is low. Typical complexity for an online estimator would fall in the 15 to 50 region.

Fig. 7 reveals that as the order increases, the one-step prediction error decreases. Thus, the error in the prediction horizon tends to decrease as well. The one-step error is monotonically decreasing in magnitude because if the order is increased and the new weights were held to be zero, we would have the same error of the lower order case. Therefore, the one-step error would never increase with increasing adaptive filter order. However, minimizing the one-step error does not necessarily correspond to minimizing the error at some arbitrary time in the prediction horizon.

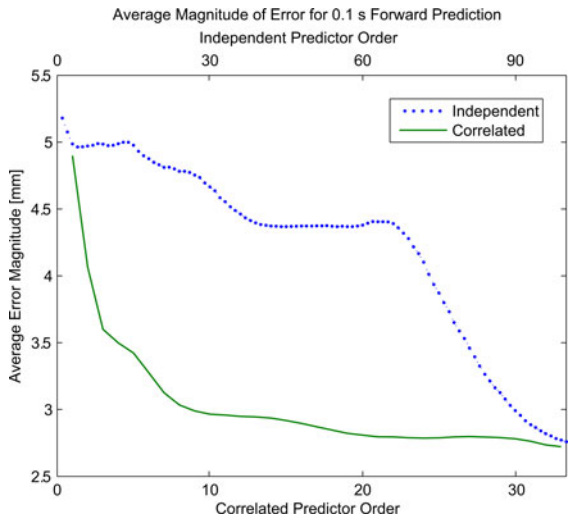

Fig. 7. Comparison plot for independent and correlated signal predictions. The independent predictor complexity is equivalent to the order of adaptive filter used for RLS predictors for each axis. Correlated predictor complexity is three times the adaptive filter order. The trend of the plot is that for the computational effort required, accounting for correlation between signals yields better results. The x-axis at the bottom shows the correlated predictor order. The x-axis at the top shows the independent predictor order. The axes are scaled to align filters with same computational complexity on both axes.

B. Prediction Error Within the Time Window

Section VII-A studied the effect of predictor order on the prediction error for a fixed amount of time in the future. However, the prediction error varies based upon how far it is predicted into the future. Fig. 8 shows the error across the prediction horizon of the correlated predictions for several complexities—as calculated in Section VII-A. The figure is created in the same manner as described in Section VII-A.

The behavior of these plots appears to be linear for times in the immediate future, and holds particularly well for the lower complexity cases. The monotonically increasing error with lead time displayed in this plot reflects that the quality of the estimation decreases as you attempt to estimate further into the future. This generalization will be useful for allowing the predictive controller to properly weight the estimates in the horizon when calculating the control law.

C. Sampling Time

Sampling time is an important parameter for the performance of the estimator. A higher sampling rate results in more of the higher frequency information to be incorporated by the estimator. Running at a lower sampling rate means that there is a larger numerical difference between samples, which is

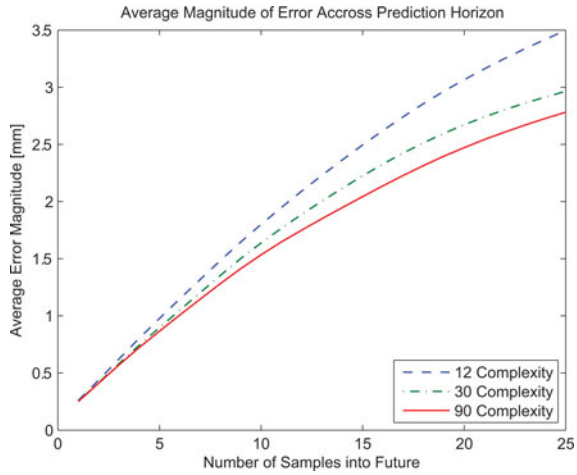

Fig. 8. Plot showing how the magnitude of the error varies throughout the prediction horizon for the correlated predictor. The data are processed at a sampling rate of 257 Hz. The prediction horizon used in the model predictive controller would correspond to seven samples in length at this frequency. Additional points are displayed to illustrate the trend.

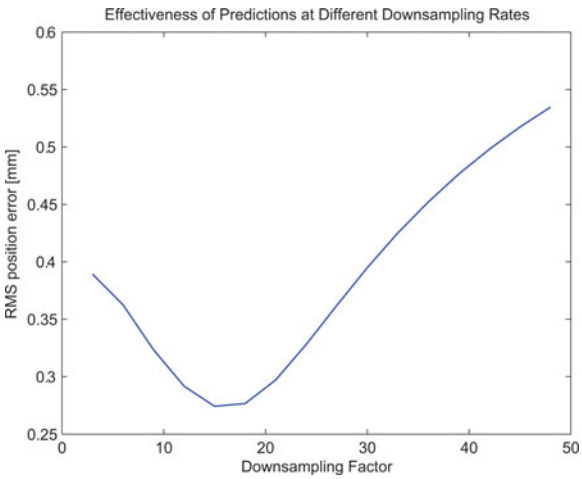

Fig. 9. Predictions can be made from a downsampled version of the 2-kHz POI signal. High-frequency processing lends to problems with numerical accuracy, and low-frequency processing can misrepresent the dynamics by excessive interpolation. This plot illustrates this tradeoff and suggests an optimal downsampling factor of 15 for the predictor.

important in the finite precision implementation. In addition, to predict over a fixed length horizon at a lower sampling rate, fewer iterations of the predictor need to be computed. Finally, for a predictor of a fixed length, the sampling rate corresponds to how much time is between each sample—translating to how far back the system has memory. In Fig. 8, the predictor order translates to the number of past observations available to the predictor, whereas the sampling rate corresponds to the spacing between those points.

The control algorithm used by the 3-DOF robotic test bed run at a sampling rate of 2 kHz. This is well above the Nyquist rate for heart motion signal which, for 100 beats/min and allowing for six harmonics, is about 20 Hz. The RMS position error versus sampling rate for the 16th order one-step predictor are plotted in Fig. 9. From this plot, it appears the ideal downsampling rate in this controller is 15—corresponding to a processing frequency of 133 Hz. This optimal value is a tradeoff between the numerical problems associated with calculating predictions using a finite number of samples at high sampling rates and the inaccuracy caused by interpolation and aliasing.

VIII. Experiments and Results

A. Three-Degrees-of-Freedom Robotic Test Bed

The proposed estimation algorithms were tested on a PHANToM Premium 1.5A haptic device, which is a 3-DOF robotic system. The nonlinearities of the system (i.e., gravitational effects, joint frictions, and Coriolis and centrifugal forces) were canceled independently from the controller. In order to maintain the accuracy of the experiments, the robotic test bed was brought to a selected home (zero) position, in the center of its workspace (more details can be found in [23]), before each experiment.

The controller used by Bebek and Cavusoglu [5] was modified to include the new prediction algorithms. The trials used the prerecorded heart motion data described in Section III. The robot was adjusted to follow the combined motion of heartbeat and breathing. The system used online streaming position data in place of real-time measurements. The controller was implemented in xPC Target and run in real time with a sampling time of 0.5 ms on a Intel Xeon 2.33 GHz Core PC. The linearized robot model was controlled using RHMPC. The RHMPC was formulated to track the horizon estimate weighted by a quadratic objective function. The encoder positions on the PHANToM were recorded, and these positions were transformed into end-effector positions. The reported RMS errors were calculated from the difference between the prerecorded target point and the actual end-effector position calculated from joint angles.

B. Simulation and Experimental Results

The same control method and reference data were used while running simulations and experiments. During the trials, a 16th-order correlated signal one-step estimator and a 10th order generalized estimator predicting four different future points in the 25-ms horizon were used and quadratic interpolation was accounted for the intermittent points. The 25-ms horizon corresponds to 50 points in the future. This length of horizon was chosen for the optimum error/performance ratio [5]. The predictors were downsampled by a factor of 15, processing observations that were 7.5 ms apart. The experiments were carried out using two different constant heart rate data and four different varying heart rate data.

Experiments were run ten times with the estimation algorithms and again with the actual heart motion data as future signal reference for the prediction horizon. The latter case represents a "perfect" estimation, providing a performance base of the robotic system's capability. It was noted that the deviation between the trials had been very small. Among these results, the maximum values for the *end-effector RMS and maximum position errors in millimeters* in 3-D, and *RMS control effort in*

TABLE I
SIMULATION RESULTS FOR END-EFFECTOR TRACKING

(a) RMS POSITION ERROR AND MAX POSITION ERROR FOR THE CONTROL ALGORITHMS

End-effector Tracking Results	RMS Position Error [mm] (Maximum Position Error [mm])					
Heart Rate	Fixed		Varying			
DataSet	Animal 1	Animal 2	Animal 1	Animal 3	Animal 1	Animal 3
Crystal Position	Top	Top	Top	Top	Side	Side
Peak-to-peak amplitude of POI motion [mm]	12.19	8.39	13.75	7.43	13.39	7.96
Receding Horizon Model Predictive Controller with Exact Reference Information	0.488 (1.428)	0.237 (1.236)	0.231 (0.777)	0.197 (0.650)	0.194 (1.542)	0.231 (1.033)
Receding Horizon Model Predictive Controller with One-Step Adaptive Filter Estimation	0.524 (1.953)	0.255 (1.460)	0.247 (1.098)	0.206 (0.917)	0.201 (2.163)	0.237 (1.195)
Receding Horizon Model Predictive Controller with Generalized Adaptive Filter Estimation	0.481 (1.399)	0.235 (1.173)	0.229 (0.767)	0.195 (0.861)	0.191 (1.540)	0.230 (1.059)

(b) RMS CONTROL EFFORT FOR THE CONTROL ALGORITHMS

End-effector Tracking Results	Control Effort [mNm]					
Heart Rate	Fixed		Varying			
DataSet	Animal 1	Animal 2	Animal 1	Animal 3	Animal 1	Animal 3
Crystal Position	Top	Top	Top	Top	Side	Side
Receding Horizon Model Predictive Controller with Exact Reference Information	18.873	14.589	16.647	11.719	13.675	14.137
Receding Horizon Model Predictive Controller with One-Step Adaptive Filter Estimation	26.685	21.801	37.991	18.010	30.402	20.027
Receding Horizon Model Predictive Controller with Generalized Adaptive Filter Estimation	19.865	17.294	16.786	12.242	13.840	13.909

TABLE II
EXPERIMENTAL RESULTS FOR END-EFFECTOR TRACKING

(a) RMS POSITION ERROR AND MAX POSITION ERROR FOR THE CONTROL ALGORITHMS

End-effector Tracking Results	RMS Position Error [mm] (Maximum Position Error [mm])					
Heart Rate	Fixed		Varying			
DataSet	Animal 1	Animal 2	Animal 1	Animal 3	Animal 1	Animal 3
Crystal Position	Top	Top	Top	Top	Side	Side
Peak-to-peak amplitude of POI motion [mm]	12.19	8.39	13.75	7.43	13.39	7.96
Receding Horizon Model Predictive Controller with Exact Reference Information	0.344 (1.238)	0.162 (0.912)	0.163 (0.780)	0.171 (0.559)	0.161 (0.538)	0.165 (0.906)
Receding Horizon Model Predictive Controller with One-Step Adaptive Filter Estimation	0.404 (2.236)	0.176 (1.395)	0.181 (1.576)	0.199 (1.084)	0.173 (0.960)	0.188 (1.022)
Receding Horizon Model Predictive Controller with Generalized Adaptive Filter Estimation	0.351 (1.291)	0.174 (1.022)	0.168 (0.827)	0.178 (0.615)	0.164 (0.572)	0.167 (0.972)

(b) RMS CONTROL EFFORT FOR THE CONTROL ALGORITHMS

End-effector Tracking Results	Control Effort [mNm]					
Heart Rate	Fixed		Varying			
DataSet	Animal 1	Animal 2	Animal 1	Animal 3	Animal 1	Animal 3
Crystal Position	Top	Top	Top	Top	Side	Side
Receding Horizon Model Predictive Controller with Exact Reference Information	54.379	28.512	25.350	21.593	24.390	27.260
Receding Horizon Model Predictive Controller with One-Step Adaptive Filter Estimation	55.686	33.785	46.820	24.346	52.640	29.592
Receding Horizon Model Predictive Controller with Generalized Adaptive Filter Estimation	54.948	29.699	25.760	22.082	24.635	27.830

millinewton meters are summarized in Table I for simulations and in Table II for experiments to project the worst cases.[1] The experimental data were collected from three calves via *in vivo* clinical experiments. From first and third calves, both constant heart rate and varying heart rate motion data were collected. Heart rate variation was generated by employing an artificial pacemaker. Heart rate was constant in the data from second calf. The results shown in Tables I and II are grouped with respect to type of the heart rate data collected from the animals. The position of the sonomicrometer crystal on the heart surface,

[1]Simulation and Experimental Results: The fixed heart rate data from animal 1 is 235 s long with a sampling rate of 404 Hz and from animal 2 is 472 s long with a sampling rate of 257 Hz. The sampling rate of all datasets with varying heart rate are 404 Hz. The duration of the varying heart rate data from animal 1 is 251 s for top position and 250 s for the side position. The duration for the varying heart from animal 3 is 200 s for top position and 140 s for side position.

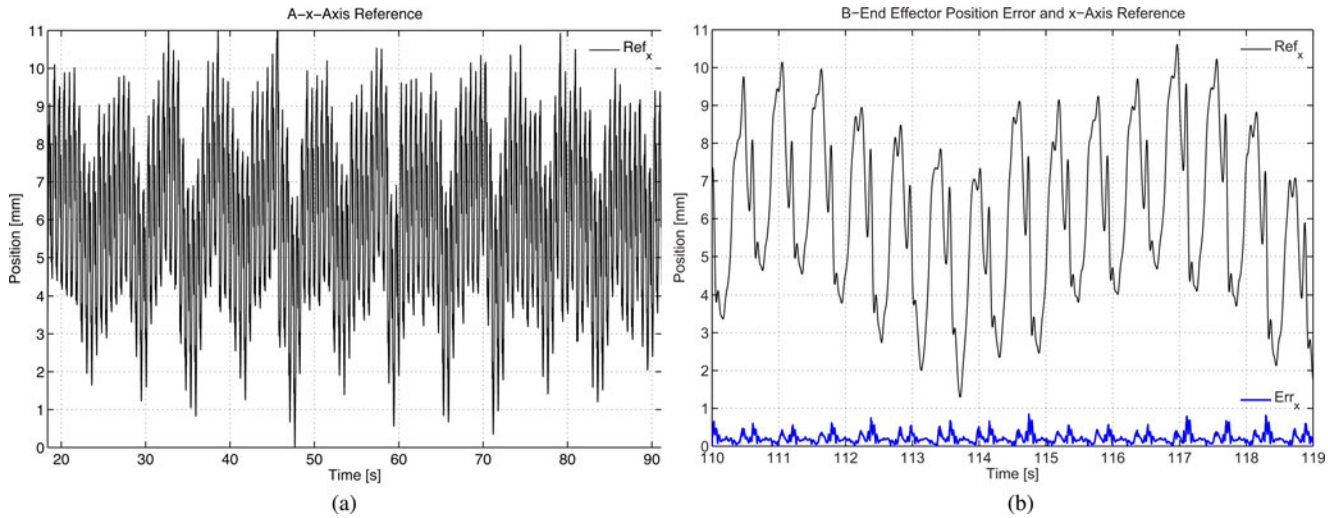

Fig. 10. Tracking results for 157-s constant heart rate heart motion data in two different scales with RHMPC with one-step adaptive filter estimation. (a) reference signal for the x-axis. (b) Magnitude of the end-effector error (below) superimposed with the reference signal for the x-axis.

which are called "top" and "side," respectively, and peak-to-peak amplitude of the heart motion are also stated.

Tracking results for a constant heart rate data with the one-step estimator in two different scales are shown in Fig. 10 and results for varying heart rate data with the generalized adaptive filter estimation are shown in Fig. 11. When Figs. 10(a) and 11(a) are compared, the variations in the heart rate can be observed from the pattern of the reference signal for x-axis in Fig. 11(A). In Figs. 10(b) and 11(b), magnitude of the end-effector position error superimposed on the reference signal for the x-axis is shown. We believe that the maximum error values are affected from the noise in the data sensor as it is unlikely that the POI on the heart is capable of moving 5 mm in a few milliseconds. The data have been kept as-is, without applying any filtering to eliminate these jumps in the sensor measurements as currently we do not have an independent set of sensor measurements (such as from a vision sensor) that would confirm this conjecture.

It can be observed from the results presented in Table I that in our simulations the generalized estimator outperformed the exact heart signal in terms of RMS position error. This is likely due a combination of two factors. First, the simulation model is a linearized, reduced order model of the actual hardware. Second, the estimator has a robustness characteristic that makes its output less noisy than the actual heart data. The combination of these two factors yields better results in the linear case. However, when the experiment is performed on the hardware, the effects of the nonlinearities have become apparent and the performance of the estimator-driven controller decreases. It should be noted that although the simulation provides valuable insight about the effectiveness of the controller, the experimental trials are the best indicator of performance.

When the tracking results of the adaptive predictors are compared with each other, the generalized predictor outperforms the one-step predictor in all simulations and all experiments.

From the results presented in Table II, it can be observed that, in the experiments the controller with exact heart signal reference performs better than the one-step estimator and the generalized estimator in term RMS end-effector error for both constant heart rate data and varying heart rate data. Maximum error and control effort results for the exact heart signal are also smaller than the tracking results of one-step and generalized estimators because the controller with exact heart signal reference represents the perfect estimation for heart motion tracking.

C. Comparative Study

At this point, it would be informative to compare the presented tracking results with the reported values in the literature.

Ginhoux *et al.* [8] used motion canceling through prediction of future heart motion using high-speed visual servoing with a model predictive controller. Their results indicated a tracking error variance on the order of 6 to 7 pixels (approximately 1.5–1.75 mm calculated from the 40 pixel/cm resolution reported in [8]) in each direction of a 3-DOF tracking task. Although it yielded better results than earlier studies using vision systems, the error was still very large to perform heart surgery.

Bebek and Cavusoglu used the past heartbeat cycle motion data, synchronized with the ECG data, in their estimation algorithms. They achieved 0.682-mm RMS end-effector position error on a 3-DOF robotic test-bed system [5].

Yuen *et al.* used an EKF algorithm with a quasi-periodic motion model to predict the path of mitral valve motion in order to compensate the time delay occurred from the 3-D ultrasound (3DUS) measurements. They achieved 1.15 ± 0.004 mm RMS tracking error for a 1-DOF motion compensation instrument (MCI) in an *in vitro* 3DUS-guided servoing test. They stated that employing the EKF-based predictor in time-delay compensation restores the tracking performance of MCI to baseline tracking conditions in cases of delay. They reported that the EKF gives better predictions than the AR filtering algorithms and last cycle method used by Bebek and Cavusoglu [5] in the presence of high noise and heart rate variability. Yuen *et al.* concluded that since the EKF explicitly models the quasi-periodic motion of

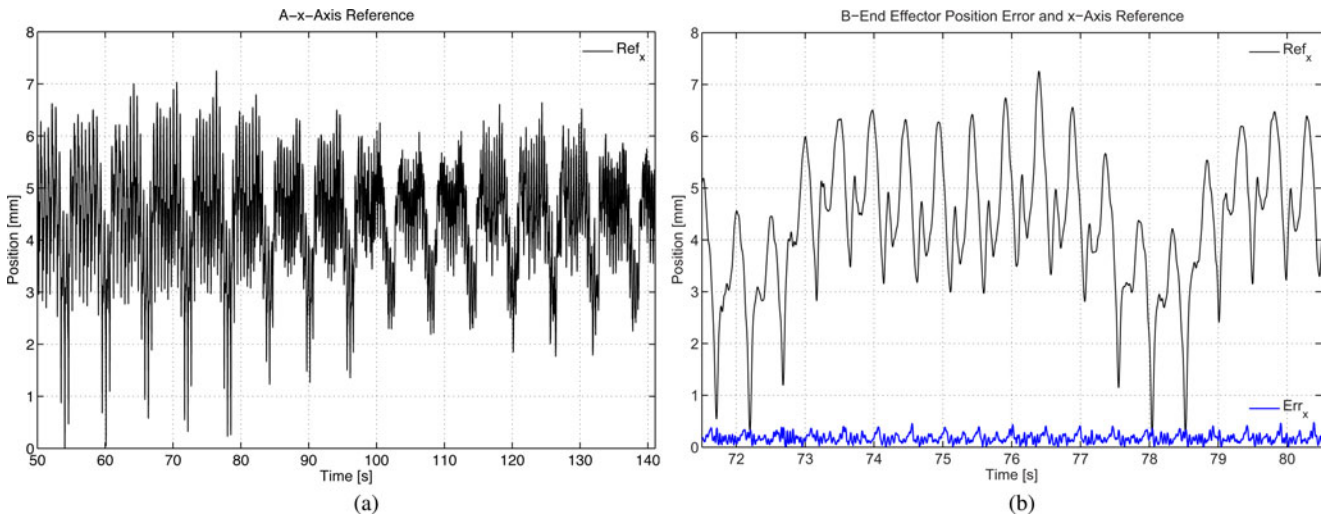

Fig. 11. Tracking results for 200-s varying heart rate heart motion data in two different scales with RHMPC with generalized adaptive filter estimation. (a) reference signal for the x-axis. (b) Magnitude of the end-effector error (below) superimposed with the reference signal for the x-axis.

the heart, it can adjust to rapid changes in heart rate better than other algorithms [17].

An essential part of this research is to evaluate and improve the performance of adaptive prediction algorithms under heart rate variations. Thus, it is crucial to compare the tracking performances of the proposed one-step and the generalized predictors with the EKF algorithm developed by Yuen *et al.* [17]. For this purpose, the same hardware experiment described in Section VIII-B was repeated by employing the estimates generated by the EKF in the RHMPC controller. The experimental results of these experiments, which include end-effector RMS position errors and maximum end-effector position errors, are presented in Table III. The results for RLS-based adaptive algorithms from Table II-A are also presented in Table III for comparison. The results of the experiments showed that the proposed adaptive algorithms outperformed the EKF-based algorithm in terms of tracking performance.

For these experiments, a 3-D harmonic model EKF was employed. EKF was implemented as described in [17]. The parameters were specifically tuned to minimize RMS end-effector tracking error. Initial state was computed in the same way as explained in [17]. State transition matrix $\boldsymbol{F}$ was same as in [17]. The process noise covariance $\boldsymbol{Q}$ is a diagonal matrix with all values set to 10^{-3}, except for q_w corresponding to $w(t)$, which was set to $5 \times 10^{-3}(\text{rad/s})^2$. The initial state estimate covariance was set to $\boldsymbol{P}(T|T) = \text{diag}[\sigma_r^2/N, \sigma_1^2, \sigma_1^2/2^2, \ldots, \sigma_1^2/m^2, \sigma_\omega^2, 10^{-3}\,\text{rad}^2, \ldots, 10^{-3}\text{rad}^2]$, where $m = 5$ is the number of harmonics, and N is the number of initialization points, corresponding to number of measurements in 10 s. Standard deviation of the measurement noise was set to $\sigma_r = 0.3\,\text{mm}$, which is very close to the accuracy of sonomicrometer (250 μm). Remaining parameters were set to $\sigma_1^2 = 1\,\text{mm}^2$ and $\sigma_\omega^2 = 0.10\,(\text{rad/s})^2$.

Simulation studies similar to the ones in [17] were conducted to compare the prediction performances of the one-step predictor, generalized predictor EKF, and last-cycle methods, in order to further investigate the tracking results presented in Table III. In these simulations, the prediction performances of the algorithms were explored in the presence of measurement noise and heart rate variations.

In the first simulation study, the effect of measurement noise on the predictor performance on a constant heart rate motion data was evaluated. The motion data of POI on heart surface were downsampled to 28 Hz and corrupted by a additive zero-mean Gaussian noise with standard deviation $0.3 \leq \sigma_r \leq 3\,\text{mm}$ to match the conditions used in [17]. Similarly, the performance was evaluated for one-step ahead prediction for a 10 s of data after 30 s of initialization time for each predictor.

The EKF predictor was also implemented with the parameters presented in that study for comparison. (These parameters were different from the EKF parameters used in experiments that are presented earlier.) The RMS measurement error for each predictor obtained by averaging across 100 Monte Carlo trials is shown in Fig. 12. Results show that EKF performs the best in the presence of high-measurement noise when compared with the other algorithms.

In the second simulation study, the performance of the predictors in the presence of variations in heart rate were evaluated. The motion data were constructed similar to the way described in [17]. First part of the data included heart motion at a constant rate of 103 beats/min with a duration of 30 s, and the second part was a 10 s of motion data at a different heart rate $(103 + \Delta\text{HR}$ beats/min), which was varied between $-10 \leq \Delta\,\text{HR} \leq 10$ beats/min. The motion data with varying heart rate were generated by compression and dilation of the trajectory of POI on heart surface. Heart motion data were again downsampled to 28 Hz and corrupted with additive white Gaussian noise with $\sigma_R = 1.30$ mm. The performance of the predictors were evaluated only for the motion with varying heart rate and for the one-step ahead predictions. The RMS errors were computed for 100 Monte Carlo trials, and EKF was implemented again with the parameters given in [17]. The results presented in Fig. 13 show that EKF yielded better results than the AR filtering algorithms and last cycle method. One step and generalized predictors

TABLE III
EXPERIMENTAL RESULTS FOR END-EFFECTOR TRACKING: RMS END-EFFECTOR AND MAXIMUM POSITION ERRORS FOR THE CONTROLLER WITH EKF PREDICTOR

End-effector Tracking Results	RMS Position Error [mm] (Maximum Position Error [mm])					
Heart Rate	Fixed		Varying			
DataSet	Animal 1	Animal 2	Animal 1	Animal 3	Animal 1	Animal 3
Crystal Position	Top	Top	Top	Top	Side	Side
Receding Horizon Model Predictive Controller with Exact Reference Information	0.344 (1.238)	0.162 (0.912)	0.163 (0.780)	0.171 (0.559)	0.161 (0.538)	0.165 (0.906)
Receding Horizon Model Predictive Controller with One-Step Adaptive Filter Estimation	0.404 (2.236)	0.176 (1.395)	0.181 (1.576)	0.199 (1.084)	0.173 (0.960)	0.188 (1.022)
Receding Horizon Model Predictive Controller with Generalized Adaptive Filter Estimation	0.351 (1.291)	0.174 (1.022)	0.168 (0.827)	0.178 (0.615)	0.164 (0.572)	0.167 (0.972)
Receding Horizon Model Predictive Controller with EKF Estimation	1.148 (5.157)	0.386 (2.863)	0.515 (3.006)	0.523 (2.859)	0.433 (2.475)	0.449 (2.796)

The results for RLS-based adaptive algorithms from Table II-A are also presented for comparison.

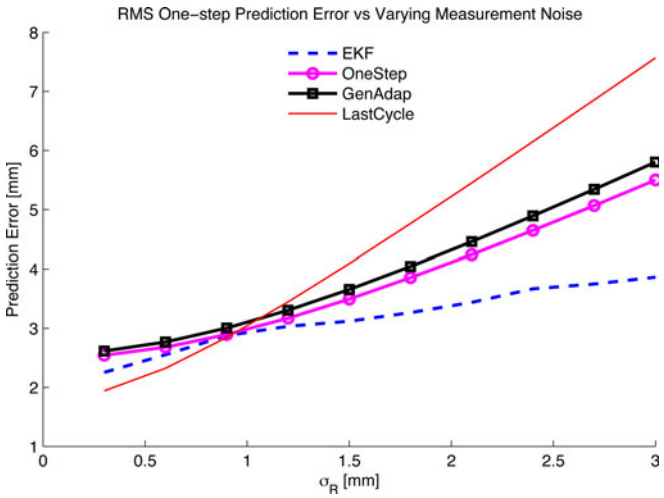

Fig. 12. Plot showing the RMS prediction error results for a parametric simulation study where the predictors are tested in the presence for varying measurement noise at a sampling rate of 28 Hz.

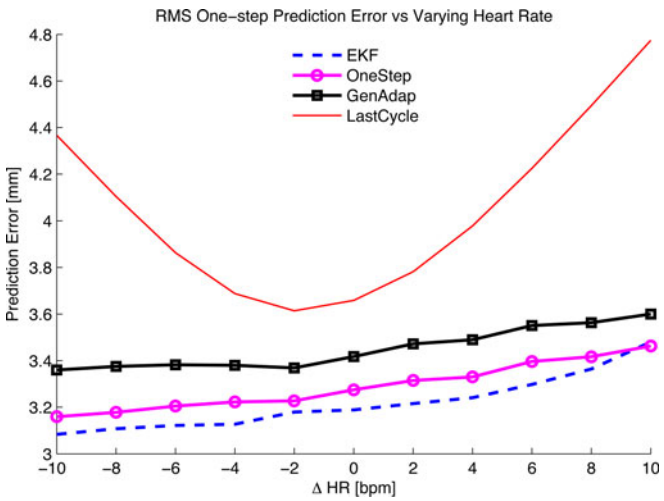

Fig. 13. Plot showing the RMS prediction error results for a parametric simulation study where the predictors are tested in the presence for varying heart rate at a sampling rate of 28 Hz.

provided similar results with former giving slightly better results. Finally, the last cycle method gave comparable results to adaptive predictors when variation in heart rate is small, yet the prediction error increases significantly when ΔHR increases.

The comparison between the algorithms presented in [17] was based on one-step prediction performances in simulation, whereas the results reported in Table III compare algorithms in terms of the tracking performances on a hardware test bed. Results from the two simulation studies presented earlier agree with the results reported in [17], indicating that EKF produces better one-step predictions than the adaptive algorithms and the last cycle method in the presence of high measurement noise and variations in heart rate at a sampling rate of 28 Hz. However, a better one-step prediction performance does not necessarily translate to a better tracking performance because of the high order and nonlinear dynamics of the robotic platform and the controllers employed.

IX. DISCUSSION

The presented tracking results show that the model predictive controller with the generalized estimator and the exact reference data performed equally well, which indicates that the main cause of error is no longer the prediction but the performance limitations of the robot and controller. It is important to note that the results also need to be validated *in vivo*, which were the case in [8] and [17]. This would also evaluate the robustness of the adaptive prediction methods with respect to changing heart statistics during CABG surgery.

The algorithms should be also tested on an actual robotic surgical system for further validation. This system should have lightweight links, low inertia design, and low-friction actuation system for tracking the heart with sufficient motion and speed. Although the test-bed system used in this study captures many desirable features, such as high bandwidth and low inertia, it has some shortcomings. Such a realistic prototype with desirable characteristics is being developed [24], and evaluation on this prototype remains as future work.

The discussion regarding the described adaptive predictors is extended below. The following two points will further enlighten

their analysis. In Section VII-C, it is observed that there is an optimum sampling rate, which yields the best performance. The assessment for the effect of sampling rate on prediction accuracy is performed under a fixed filter order. Using a higher filter order requires a higher sampling rate, which can decrease the amount of noise in the estimator. However, this increases computational load significantly, which is not desirable. Therefore, for a given filter order, there is a tradeoff between the amount of noise in the estimator and the computational load, which results from the choice of sampling rate. RMS position error obtained by filter shows that there appears to be an optimal frequency, which balances this tradeoff.

Noise of the measurements is another issue to be considered in the implementation of predictors. The main source of error in the sonomicrometry system is the crystal geometry. The sound wave is received by the leading edge of the crystal surface. Thus, the orientation of the crystals might affect the measured distance. This error might be approximated by a white noise [18]. Although there might be other sources of noise, white noise assumption is satisfactory at this point.

From all of the position tracking sensors, extracting accurate and precise position information of the heart is required for precise motion canceling performance, and therefore, an important prerequisite for proper working of the control algorithms. In this manner, sensor systems used for tracking in beating heart surgery are crucial. Earlier studies in canceling beating motion with robotic-assisted tools used vision-based and ultrasound-based sensory systems to measure heart motion. The selection of the sensor systems for use in beating heart surgery [4], [6], [11], [12], [17], [20], [25]–[27] is critical and deserves a detailed comparative study. However, such a comparison is outside the scope of this paper.

When the robotic platform contacts with the heart, heart dynamics are likely to change, arrthymias might occur and robot dynamics might alter significantly. Additionally, the motion of the heart might dampen locally as a result of this contact. Therefore, the control scheme for surgical tasks involving a contact between the robot and heart requires further investigation. Employing a force feedback control is a feasible approach to solve such issues as explained by Cagneau *et al.* [28]. Cagneau *et al.* used a force sensor equipped robot designed for minimally invasive surgery in [29] to compensate for physiological motions in surgical tasks involving tissue contact. However, the proposed force feedback controller did not perform effective motion compensation. Yuen *et al.* [30] used an optical force sensor equipped motion compensation instrument to follow rapid motion of mitral valve annulus. Their proposed force controller that employs feedforward target motion information enables the robotic system to operate at the bandwidth of the heart motion while simultaneously ensuring damping and providing good disturbance rejection. However, the provided system would not perform well in the cases of high heart rate variability and arrhythmia as the tissue motion would not follow the feedforward model predictions provided by the EKF.

Another point to discuss is the effect of using artificial pacemakers on the heart motion dynamics. Currently, this effect is unknown, and it remains to be studied as future work.

X. Conclusion

In this paper, a one-step and a generalized estimator for predicting the horizon estimate for the model predictive controller are presented. Three different sets of experiments are performed with constant heart rate and varying heart rate to evaluate the performance of the proposed algorithms. The experimental RMS errors on the order of 0.160–0.350 mm obtained using the generalized estimator represent a significant improvement in tracking performance compared with earlier studies. Therefore, the estimation of future POI motion is no longer the bottleneck in the heartbeat motion tracking since the necessary amount of RMS tracking error on the order of 100–250 μm is achieved.

Furthermore, the results showed that if the heart statistics change, then adaptive predictors are able to adjust to these changes sufficiently quickly and yield good tracking results. However, if the statistics change abruptly and significantly, such as in an arrhythmia or a contact between the robotic platform and the heart, actions must be taken to minimize the effect of poor predictions.

Another way to improve tracking quality is to incorporate other types of data into the estimation scheme. One such possibility is to include the electrocardiogram (ECG) signal into the observations. This way, the predictor is able to use the electrical signals that activate heart contraction in order to improve the prediction as in [5]. This may improve performance during heart contractions, when rapid POI motion occurs.

Future works also include multisensor fusion, where complementary and redundant sensors will be used for superior performance and safety, e.g., a vision-based sensor system could be used as a secondary sensor for the *in vivo* validation of the proposed concept. Merging the sensor data from multiple position sources would increase accuracy of the motion estimation and improve tracking results. Adding more mechanical sensors that measure heart motion would improve the measurement precision and help to resolve the calibration problems of the sonomicrometry system.

References

[1] A. L. Trejos, S. E. Salcudean, F. Sassani, and S. Lichtenstein, "On the feasibility of a moving support for surgery on the beating heart," in *Proc. Med. Image Comput. Comput.-Assist. Interventions*, Cambridge, U.K., Sep. 1999, pp. 1088–1097.

[2] M. F. Newman, J. L. Kirchner, B. Phillips-Bute, V. Gaver, H. Grocott, R. H. Jones, D. B. Mark, J. G. Reves, and J. A. Blumenthal, "Longitudinal assessment of neurocognitive function after coronary-artery bypass surgery," *New England J. Med.*, vol. 344, no. 6, pp. 395–402, Feb. 2001.

[3] M. Lemma, A. Mangini, A. Redaelli, and F. Acocella, "Do cardiac stabilizers really stabilize? Experimental quantitative analysis of mechanical stabilization," *Interact. CardioVascular Thoracic Surg.*, no. 4, pp. 222–226, Mar. 2005.

[4] Y. Nakamura, K. Kishi, and H. Kawakami, "Heartbeat synchronization for robotic cardiac surgery," in *Proc. IEEE Int. Conf. Robot. Autom.*, vol. 2, Seoul, Korea, May 2001, pp. 2014–2019.

[5] O. Bebek and M. C. Cavusoglu, "Intelligent control algorithms for robotic-assisted beating heart surgery," *IEEE Trans. Robotics*, vol. 23, no. 3, pp. 468–480, Jun. 2007.

[6] M. C. Cavusoglu, J. Rotella, W. S. Newman, S. Choi, J. Ustin, and S. S. Sastry, "Control algorithms for active relative motion cancelling for robotic assisted off-pump coronary artery bypass graft surgery," in *Proc. 12th Int. Conf. Adv. Robot.*, Seattle, WA, Jul. 2005, pp. 431–436.

[7] J. Rotella, "Predictive tracking of quasi periodic signals for active relative motion cancellation in robotic assisted coronary artery bypass graft surgery," M.S. thesis, Case Western Reserve Univ., Cleveland, OH, Aug. 2004. [Online]. Available: http://vorlon.case.edu/~mcc14/research/papers/JasonRotellaMS2004.pdf
[8] R. Ginhoux, J. A. Gangloff, M. F. DeMathelin, L. Soler, J. Leroy, M. M. A. Sanchez, and J. Marescaux, "Active filtering of physiological motion in robotized surgery using predictive control," *IEEE Trans. Robotic.*, vol. 21, no. 1, pp. 67–79, Feb. 2005.
[9] T. Franke, O. Bebek, and M. C. Cavusoglu, "Improved prediction of heart motion using an adaptive filter for robot assisted beating heart surgery," in *Proc. IEEE/RSJ Int. Conf. Intell. Robots Syst.*, San Diego, CA, Oct./Nov. 2007, pp. 509–515.
[10] T. Franke, O. Bebek, and M. C. Cavusoglu, "Prediction of heartbeat motion with a generalized adaptive filter," in *Proc. Int. Conf. Robot. Autom.*, Pasadena, CA, May 2008, pp. 2916–2921.
[11] T. Ortmaier, M. Groeger, D. H. Boehm, V. Falk, and G. Hirzinger, "Motion estimation in beating heart surgery," *IEEE Trans. Biomed. Eng.*, vol. 52, no. 10, pp. 1729–1740, Oct. 2005.
[12] T. Bader, A. Wiedemann, K. Roberts, and U. D. Hanebeck, "Model-based motion estimation of elastic surfaces for minimally invasive cardiac surgery," in *Proc. Int. Conf. Robot. Autom.*, Rome, Italy, Apr. 2007, pp. 2261–2266.
[13] R. Richa, A. P. L. Bo, and P. Poignet, "Motion prediction for tracking the beating heart," in *Proc. Annu. Int. Conf. Eng. Med. Biol. Soc.*, Vancouver, BC, Canada, Aug. 2008, pp. 3261–3264.
[14] R. Richa, A. P. Bó, and P. Poignet, "Towards robust 3D visual tracking for motion compensation in beating heart surgery," *Med. Image Anal.*, vol. 15, pp. 302–315, 2011.
[15] W. Bachta, P. Renaud, L. Cuvillon, E. Laroche, A. Forgione, and J. Gangloff, "Motion prediction for computer-assisted beating heart surgery," *IEEE Trans. Biomed. Eng.*, vol. 56, no. 11, pp. 2551–2563, 2009.
[16] S. G. Yuen, P. M. Novotny, and R. D. Howe, "Quasiperiodic predictive filtering for robot-assisted beating heart surgery," in *Proc. Int. Conf. Robot. Autom.*, Pasadena, CA, May 2008, pp. 3875–3880.
[17] S. G. Yuen, D. T. Kettler, P. M. Novotny, R. D. Plowes, and R. D. Howe, "Robotic motion compensation for beating heart intracardiac surgery," *Int. J. Robot. Res.*, vol. 28, no. 10, pp. 1355–1372, Oct. 2009.
[18] M. B. Ratcliffe, K. B. Gupta, J. T. Streicher, E. B. Savage, D. K. Bogen, and J. L. H. Edmunds, "Use of sonomicrometry and multidimensional scaling to determine the three-dimensional coordinates of multiple cardiac locations: Feasibility and initial implementation," *IEEE Trans. Biomed. Eng.*, vol. 42, no. 6, pp. 587–598, Jun. 1995.
[19] G. Kalogeros, *Sales and Marketing Director*, Sonometrics Corp., London, ON, Canada, Apr. 25, 2006.
[20] M. Groeger, T. Ortmaier, W. Sepp, and G. Hirzinger, "Tracking local motion on the beating heart," *Proc. SPIE*, vol. 4681, pp. 233–241, Feb. 2002.
[21] W. Wei, *Time Series Analysis—Univariate and Multivariate Methods*. New York: Addison-Wesley, 1990.
[22] S. Haykin, *Adaptive Filter Theory*, 4th ed. Upper Saddle River, NJ: Prentice–Hall, 2001.
[23] M. C. Cavusoglu, D. Feygin, and F. Tendick, "A critical study of the mechanical and electrical properties of the phantom haptic interface and improvements for high performance control," *Presence: Teleoperators Virtual Environ.*, vol. 11, no. 6, pp. 555–568, 2002.
[24] T. Liu, "Design and prototyping of a three degrees of freedom robotic wrist mechanism for a robotic surgery system," M.S. thesis, Case Western Reserve Univ., Cleveland, OH, Jan. 2011. [Online]. Available: http://etd.ohiolink.edu/view.cgi?acc_num=case1283538593
[25] A. Thakral, J. Wallace, D. Tomlin, N. Seth, and N. V. Thakor, "Surgical motion adaptive robotic technology (S.M.A.R.T.): Taking the motion out of physiological motion," in *Proc. 4th Int. Conf. Med. Image Comput. Comput.-Assisted Intervention*, Utrecht, The Netherlands, Oct. 2001, pp. 317–325.
[26] M. L. Koransky, M. L. Tavana, A. Yamaguchi, and R. Robbins, "Quantification of mechanical stabilization for the performance of offpump coronary artery surgery," presented at the *Proc. Meet. Int. Soc. Minimally Invasive Cardiac Surg.*, Munich, Germany, Jun. 2001.
[27] O. Bebek, "Robotic-assisted beating heart surgery," Ph.D. dissertation, Case Western Reserve Univ., Cleveland, OH, May 2008. [Online]. Available: http://etd.ohiolink.edu/view.cgi?acc_num=case1201289393
[28] B. Cagneau, N. Zemiti, D. Bellot, and G. Morel, "Physiological motion compensation in robotized surgery using force feedback control," in *Proc. Int. Conf. Robot. Autom.*, Rome, Italy, Apr. 2007, pp. 1881–1886.
[29] N. Zemiti, G. Morel, T. Ortmaier, and N. Bonnet, "Mechatronic design of a new robot for force control in minimally invasive surgery," *IEEE/ASME Trans. Mechatron.*, vol. 12, no. 2, pp. 143–153, Apr. 2007.
[30] S. G. Yuen, D. P. Perrin, N. V. Vasilyev, P. J. del Nido, and R. D. Howe, "Force tracking with feed-forward motion estimation for beating heart surgery," *IEEE Trans. Robot.*, vol. 26, no. 5, pp. 888–896, Oct. 2010.

E. Erdem Tuna (S'11) received the B.S. and M.S. degrees in electrical and electronics engineering from the Bilkent University, Ankara, Turkey, in 2009 and 2011, respectively. He is currently working toward the Ph.D. degree with the Department of Electrical Engineering and Computer Science, Case Western Reserve University, Cleveland, OH.

He was a Visiting Research Scholar with Case Western Reserve University in 2010. His research interests include control systems, medical robotics, and probabilistic state estimation.

Timothy J. Franke (S'07) received the B.S. degree in systems and control engineering from Case Western Reserve University, Cleveland, OH, in 2008, where he is working toward the Ph.D. degree with the Department of Electrical Engineering and Computer Science.

His primary research interests are focused in the area of control, particularly the application of computational methods to controller design.

Özkan Bebek (S'06–M'09) received the B.S. degree in mechanical engineering from the Middle East Technical University, Ankara, Turkey, in 2001, the M.S. degree in mechatronics from Sabanci University, Istanbul, Turkey, in 2003, and the Ph.D. degree in systems and control engineering from Case Western Reserve University, Cleveland, OH, in 2008.

He was a Senior Research Associate with the Department of Electrical Engineering and Computer Science, Case Western Reserve University, from 2008 to 2011. He is currently an Assistant Professor of mechanical engineering with Özyeğin University, Istanbul. His research interests include medical robotics, mechatronics, and control systems.

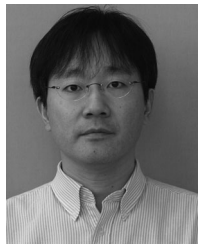

Akira Shiose is currently an Assistant Professor of cardiothoracic surgery with the University of Pittsburgh Medical Center, Pittsburgh, PA. His clinical specialty is adult and pediatric cardiac surgery and transplant surgery of the heart and lungs. His research interests include the development of innovative surgical devices for heart failure.

Kiyotaka Fukamachi is currently a Full Staff and the Head of the Section of Biomedical Devices with the Department of Biomedical Engineering, Cleveland Clinic, Cleveland, OH. He is also a Professor of molecular medicine with the Cleveland Clinic Lerner College of Medicine, Case Western Reserve University (CWRU), Cleavland, and a Professor of biomedical engineering with CWRU. Over the course of his career, he has written over 200 publications. His research interest includes making contributions to promote human health through the development of various innovative surgical and device treatments for heart failure. These include cardiac assist devices and total artificial hearts.

M. Cenk Çavuşoğlu (S'93–M'01–SM'06) received the B.S. degree in electrical and electronic engineering from the Middle East Technical University, Ankara, Turkey, in 1995 and the M.S. and Ph.D. degrees in electrical engineering and computer sciences from the University of California, Berkeley, in 1997 and 2000, respectively.

He is currently an Associate Professor of electrical engineering and computer science with Case Western Reserve University, Cleveland, OH. He was a Visiting Researcher with the INRIA Rhones-Alpes Research Center, Grenoble, France, in 1998, a Postdoctoral Researcher and Lecturer with the University of California, Berkeley (2000–2002), and a Visiting Associate Professor with Bilkent University, Ankara, (2009–2010). His research interests include robotics, systems and control theory, and human–machine interfaces, with emphasis on medical robotics, haptics, virtual environments, surgical simulation, and bio-system modeling and simulation. His current research involves applications of robotics and control engineering to biomedical and biologically inspired engineered systems.

Dr. Çavuşoğlu is currently serving as an Associate Editor of the IEEE TRANSACTIONS ON ROBOTICS, and as a Technical Editor of the IEEE/ASME TRANSACTIONS ON MECHATRONICS.